Eur. Phys. J. D **12**, 289–296 (2000)

THE EUROPEAN PHYSICAL JOURNAL D

EDP Sciences

Direct evidence of a magnetization transfer between laser-polarized xenon and protons of a cage-molecule in water*

H. Desvaux[1], T. Gautier[1], G. Le Goff[2], M. Pétro[1], and P. Berthault[1,a]

[1] Service de Chimie Moléculaire, CEA/Saclay, 91191 Gif-sur-Yvette Cedex, France
[2] Service de Physique de l'État Condensé, CEA/Saclay, 91191 Gif-sur-Yvette Cedex, France

Received 16 March 2000 and Received in final form 22 May 2000

Abstract. In a dedicated experimental setup, we directly prepare liquid-state NMR samples containing laser-polarized xenon with nuclear polarization larger than 5% at pressures up to 4 bars. Coating of the NMR tube surface allows us to increase the self-relaxation time of xenon in the gaseous phase to approximately 4.5 hours. Using a modified SPINOE pulse sequence, we present the first direct detection of a regioselective proton signal enhancement of a molecule (α-cyclodextrin) dissolved in water resulting from cross-polarization between laser-polarized xenon and protons.

PACS. 76.60.-k Nuclear magnetic resonance and relaxation – 32.80.Bx Level crossing and optical pumping – 87.15.-v Biomolecules: structure and physical properties

1 Introduction

Numerous biological processes involve gases. For instance, hemoglobin and derivatives have the role of oxygen-carriers, while other proteins such as hydrogenases act as catalysts. However their fine characterization requires to identify the active sites inside the protein, to know which are the pathways for the penetration of the gas, and to determine whether a deformation of the protein is necessary to facilitate the entrance of the gas inside its core [1]. The study of the interaction between gases and cage-molecules is also of high importance. As an example, amphiphilic cyclodextrins serve as gas sensors in piezoelectric crystals exploiting their ability to respond rapidly and in a selective way [2].

In most of the cases the cavities designed to receive the gas have an hydrophobic character. Their characterization is often difficult, including whether they are empty or contain some disordered water molecules [3,4]. The study of these pockets and cavities can be performed by NMR using small gas molecules carrying nuclear spins: hydrogen, methane, ethylene, cyclopropane, ... [5,6]. However as a consequence of their low solubility, in order to observe polarization transfer between these nuclei and some protein protons and then to build a cartography of the regions involved in the interaction, very high pressures have to be used (sometimes several hundreds of bars), which can unfold the protein [7]. The use of laser-polarized gas appears as an attractive alternative, since its very high nuclear polarization could allow one to work at moderate pressures. Among the two noble gas isotopes with a spin 1/2, for this application ^{129}Xe seems to be more promising than ^{3}He, since it exhibits a larger range of chemical shifts, its solubility is at least one order of magnitude larger than helium and it is known to be hydrophobic. Finally, in contrast to ^{3}He, it can be detected using standard broadband NMR probeheads.

Even if a large polarization enhancement is achievable, observing cross-relaxation between a laser-polarized gas and a solute molecule is difficult to achieve. This is illustrated by the rapidly increasing number of groups working with laser-polarized gas [8] compared to only two successful reports on the observation of cross-relaxation between xenon and the protons of a molecule dissolved in organic media [9,10]. The case of water, which is the most relevant for biological applications, is the most challenging, due to the low solubility of xenon whose signal is typically reduced by about a factor 30 relative to its signal in classical organic solvents such as chloroform, benzene, or cyclohexane [11]. The present article is devoted to the description of an experimental setup allowing the preparation and the use of laser-polarized xenon in liquid state NMR and to the first observation of laser-polarized $^{129}\text{Xe} \longrightarrow {}^{1}\text{H}$ cross-relaxation in water using a modified SPINOE [9] pulse sequence.

2 Materials and methods

The nuclear spin of xenon is polarized by the spin-exchange method [12–15]. For the design of our experimental setup we have taken advantage of the extended

* Dedicated to Pr. P. Sinaÿ for his 62nd birthday.

[a] e-mail: pberthault@cea.fr

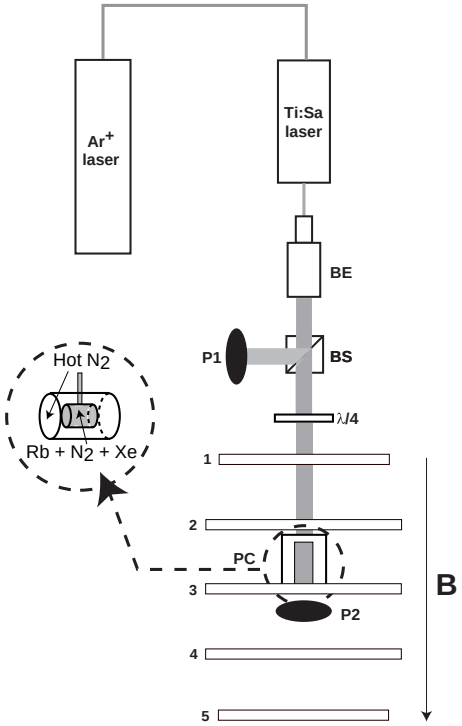

Fig. 1. Schematics of the experimental setup for optical pumping. BE: beam expander; BS: beam splitter; $\lambda/4$: quarter-wave plate; P1 and P2: power-meters. B: magnetic field collinear to the light beam. The pumping cell (PC) is constituted by a glass cylinder surrounded by another glass cylinder in which hot nitrogen is flowing. The flat surfaces of the cell are made with glass of optical quality to avoid any photon depolarization.

literature in this field [16–19]. The optics part allows a differential measurement of the absorption, taking into account the fluctuations of the laser power. Also, since we use a laser instead of a diode, low gas pressures are suitable to fit the linewidth of the laser so that, in addition to the loss of polarization by interaction with the impurities in the walls [20,21], it is necessary to avoid relaxation by B_0 magnetic field gradients during the optical pumping [22, 23]. The coils have been conceived in order to minimize these relaxation effects.

2.1 Optics

The D1 electronic transition of the rubidium atoms ($\lambda =$ 794.7 nm) is excited *via* a tunable titanium:sapphire laser (model 3900S from Spectra Physics). Pumped by an argon ionized laser (Spectra Physics Model 2040) delivering 20 W, it produces *ca.* 5 W continuous power. The light passes through a beam expander (BE), then through a beam-splitter cube (BS) (see Fig. 1). The BE serves to broaden the beam section from a diameter of about 1 mm to 25 mm in order to illuminate the whole pumping cell (PC) and to reduce the angular divergence. The BS has a double aim: it ensures that only the horizontally polarized light reaches the $\lambda/4$ plate, and it deviates the residual vertically polarized light fraction ($\sim$2%) towards a power-meter (P1). Finally, on the main optical pathway a $\lambda/4$ plate transforms the linear polarization into circular polarization. The beam is stopped after the pumping cell by a second power-meter (P2). The use of two power-meters allows a differential measurement, ensuring that the fluctuations observed on P2 are not due to variations of the laser power.

2.2 Apparatus

As depicted in Figure 1, the magnetic field in the pumping area is created by five coils. Their inner diameter is 700 mm for the three central ones, and 610 mm for the two extreme ones. The distances between two coils are 220 mm (coil 2–coil 3, coil 3–coil 4) and 195 mm (coil 1–coil 2, coil 4–coil 5). This particular design is intended to keep the maximum field homogeneity in direction in order to prevent nuclear spin relaxation due to field gradients between coils 2 and 3 and coils 3 and 4 where the pumping cell and a storage cell are respectively located. The homogeneity level created by these coils is computed to be better than 5×10^{-5} in the volume of the pumping cell and better than 2×10^{-3} in the transfer area of the polarized xenon. Supplied by a direct current of 5 A, the coils deliver a field of 56 G at the location of the pumping cell.

The pumping cell is of cylindrical shape (inner diameter 23 mm) and has a volume of 31 ml with a dark volume of about 3 ml. It is surrounded by a second cylindrical cell (outer diameter 54 mm) in which hot nitrogen is flowing. Its temperature is controlled by a Bruker VT1000 unit working with a thermocouple and a heating resistor. The complete glassware (in Pyrex) is schematized in Figure 2. Each connection between Pyrex pieces is formed by a Solv-Seal joint from Andrews Glass Co., and each connection between a Pyrex piece and a metal part is made by a Pyrex/metal weld completed by an ISO-KF joint from SVT. Teflon valves from Young Scientific Glassware Ltd are used. Regular 5 mm NMR tubes closed by a valve are purchased from Young Scientific Glassware Ltd. The glassware is continuously pumped by a turbomolecular pump from Varian Inc. This allows an average vacuum lower than 10^{-6} mbar to be obtained.

All glass surfaces are treated in the following way. First, the glassware is washed by immersion in a piranha solution (60% sulfuric acid, 40% hydrogen peroxide). Then it is dried in an oven at 390 K for about one day. Finally it is covered by a thin film of surfasil (dichlorooctamethyltetrasiloxane $C_8H_{24}Si_4O_3Cl_2$, from Pierce Chemicals), deposited by the immersion procedure using a solution of 10% v/v in dry toluene. After some hours in the oven at 390 K, the glassware is installed on the vacuum line and immediately pumped.

2.3 Chemicals

Rubidium 99.6% pure is purchased from Aldrich Chemical Inc. In a glove-box, it is introduced in the pumping cell previously coated as described above, and put under dynamic vacuum for at least 3 days. Being kept under

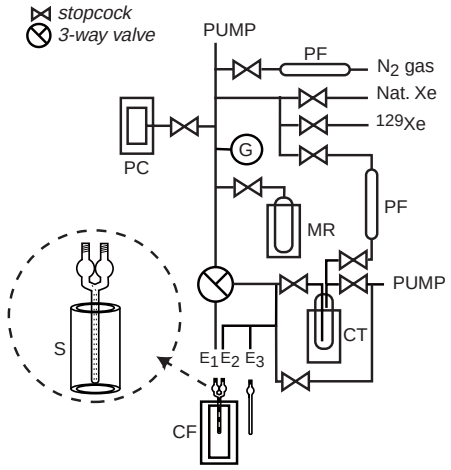

Fig. 2. Gas transfer system. The glassware can be divided into two parts. The first one serves for the introduction of the gases directly into the pumping cell (PC) or into a reservoir (MR) designed to prepare the mixture (N_2–Xe) before filling the pumping cell. The pressure is measured by a membrane gauge (G). The second part is used after optical pumping, and is designed to separate the gases and to collect laser-polarized xenon. Xenon is either directly frozen at the output E1, or in a cold-finger (CF) placed between E1 and E2. In both cases, a solenoid (S) immersed in liquid nitrogen provides a magnetic field of about 5 kG in the region where xenon is accumulated. A cold trap (CT) between the vacuum line and the pump ensures that no xenon is lost through the pump and allows us to recover xenon from the NMR tube after the experiment. Before recycling the xenon, the gas is purified through a Sertronics filter (PF) designed to trap traces of O_2 and H_2O.

pressure of nitrogen when not employed, the rubidium of the pumping cell can be used for optical pumping experiments during more than two months (representing more than fifty different experiments). This principally results from the gas-tightness of the joints and valves and from the presence of Sertronics filters (from Air-Liquide), designed to trap traces of H_2O or O_2. Xenon in natural isotopic proportions (Air-Liquide) or 96% enriched ^{129}Xe (Eurisotop) are used.

2.4 Preparation of samples containing laser-polarized xenon

The pumping cell is heated to 368 K after introduction of xenon and nitrogen. The titanium:sapphire laser output is then tuned to the wavelength corresponding to the D1 transition of rubidium. When the absorption line is found, the magnetic field is switched on. For 225 mbar nitrogen and 70 mbar xenon, about 30% of the power is transmitted in the absence of magnetic field and 93% when the field is switched on. After some minutes of optical pumping, the cell is cooled down, and xenon is transferred to the NMR tube. For this, either the gas mixture is frozen in an NMR tube located at the output E1. In this case, the three-way valve allows xenon accumulation, but only about two thirds of the polarized xenon initially present in the pumping cell are condensed in the NMR tube. Or the gas mixture reaches a cold finger located between the outputs E1 and E2. In this condition, almost all the xenon inside the pumping cell is transferred to this dewar, which is composed by a 5 mm NMR tube containing a capillary (insert of Fig. 2). Its two outputs are closed by Young's valves, allowing its displacement from the vacuum line. As this modified NMR tube does not fit into a narrow-bore magnet the polarized xenon is consequently transferred to another NMR tube either in the fringe field of the NMR magnet or at the output E3. In both cases during the xenon freezing, the NMR tube is located inside a solenoid S delivering a field of about 5 kG. The solenoid and the bottom of the NMR tube are cooled down by a tank filled by liquid nitrogen.

2.5 NMR experiments

All experiments are performed on Bruker DRX 500 or 600 spectrometers equipped with a 5 mm Bruker inverse broadband probehead or a 5 mm Nalorac broadband probehead.

The nuclear polarization of xenon is measured by comparing the signal in one scan just after optical pumping to the Boltzmann equilibrium signal of the same sample (same flip angle of the read pulse). The latter is obtained as follows. The nuclear polarization is destroyed by means of radio-frequency pulses, or more efficiently by a succession of freezing and sublimation cycles far from a magnetic field. The sample is then left to relax in the magnet for at least 5 hours, and only after is the accumulation started. The recycling delay between two acquisitions is set to 20 minutes. This delay is obviously short relative to the usual longitudinal relaxation times we measure, but we benefit from the fast diffusion of the xenon gas and the small volume covered by the NMR coil relative to the complete volume of the tube. The pressure deduced from the thermal magnetization is systematically confronted with the pressure value inside the tube obviously measured after the NMR experiments. The uncertainty of the signal enhancement factor strongly depends on the longitudinal self-relaxation time T_1^{g} and on the pressure inside the NMR tube, that is on the signal over noise ratio of the thermal equilibrium signal. According to all tests we have performed, for an NMR tube containing about 0.5 bar of xenon (typical value after one pumping cycle), the uncertainty on the signal enhancement factor is less than 10%.

The longitudinal relaxation time of gaseous xenon T_1^{g} is determined by monitoring at fixed time intervals ($\Delta =$ 10 to 15 min) the NMR signal after small flip angle rf pulses ($\theta < 6°$). The receiver gain is changed during the experiment to keep it adapted to the xenon signal level. Due to the lack of precision on the θ value, the T_1^{g} values are not corrected by the $|\log(\cos\theta)|/\Delta$ term.

3 Results

3.1 Laser-polarized xenon in the gas phase

When using dissolved laser polarized xenon in liquid state NMR, the situation can be seen as intermediate between

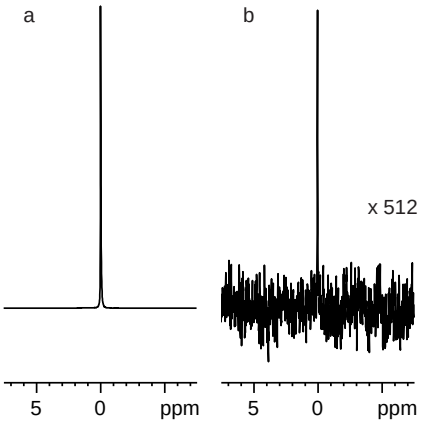

Fig. 3. Example of gaseous xenon NMR signal acquired at 11.7 T and 285 K ($P \sim 0.3$ atm). (a) Laser-polarized signal (one scan). (b) Boltzmann equilibrium signal (16 scans, receiver gain multiplied by 512). The signal enhancement is 13 200, which corresponds to a nuclear polarization of 15.3%.

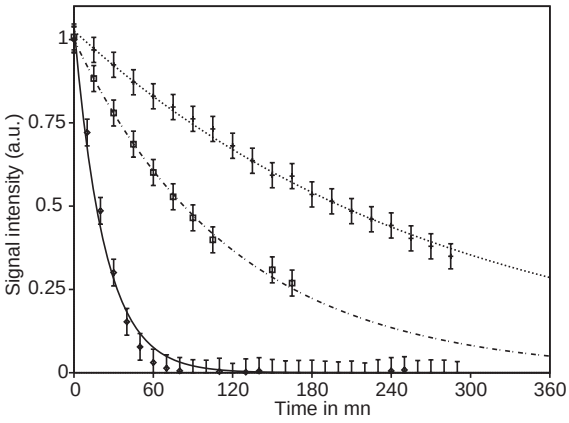

Fig. 4. Longitudinal relaxation of gaseous xenon for different treatments of the NMR tube. The longitudinal relaxation times T_1^{g} are 23±2 mn (solid line), 120±4 mn (dashed line) and 282±3 mn (dotted line) for a tube after water/ethanol/acetone washing, after treatment by the piranha solution and after coating with surfasil, respectively.

surface studies and imaging. For the former, very high polarization but a low concentration of gas are required, since the number of xenon atoms adsorbed on the surface is low [24–26]. For imaging studies where the principal need is to provide large quantities of gas, the dilution of polarized gas [27] or the use of pre-polarized gas [28,29] has been suggested. In our case, the quantity of laser-polarized gas needed is in fact limited by the pressure inside the NMR tube. The volume is about 2.4 ml for a 5 mm o.d. thin wall tube and the pressure cannot exceed 4 bars. If one uses a thick wall NMR tube, the pressure can safely be multiplied by a factor 3, but the volume is divided by about 2.4. The quantity of polarized xenon is consequently almost identical.

Using the experimental setup described in Section 2 (Materials and methods) by pumping a mixture composed of about 40 mbar of xenon and 90 mbar of nitrogen, we routinely fill the NMR tube with a pressure between 0.3 and 3 bars of xenon (according to the number of pumping cycles) at a polarization level ranging between 5 and 22% (Fig. 3). The duration of one pumping cycle is typically around 10 minutes, including the time needed to fill the cell, the heating, and then the cooling step before transfer. The effective duration of pumping required to reach the maximum polarization enhancement seems to be on the order of 3–5 min as soon as the temperature of the gas inside the cell is stabilized. As reported by Jänsch [26], decreasing the xenon fraction in the gas mixture induces an increase of the polarization. However the price to pay is a lower quantity of xenon prepared, a more difficult separation from nitrogen and a slower pumping rate.

As expected after the work of Happer [30], a significant increase in the xenon relaxation time during freezing is observed when using a magnetic field larger than 500 G. The maximum of the magnetic field provided by the five coils being around 60 G, a boost field was mandatory. After different tests we decided to resort to solenoids that present the advantage of avoiding the strong gradients associated to permanent magnets. To obtain a high static magnetic field (about 5 kG), the solenoid is directly immersed in a dewar filled with liquid nitrogen. This allows the reduction of its resistance by a factor ~ 6. Its inner diameter allows the NMR tube to be inserted. When the axis of the solenoid is correctly aligned with the NMR tube axis, we observe polarization losses smaller than 10% after freezing, (one minute in the solenoid) and heating up the sample and 39% loss observed at room temperature after being in the solenoid for a duration of 15 minutes. This shows that the condensation is a key point.

In any liquid state experiment with laser-polarized xenon, since the gaseous phase above the solution represents a reservoir of polarized xenon, the longitudinal relaxation time T_1^{g} of gaseous xenon is of key importance. Figure 4 illustrates an example of the variation of the xenon longitudinal relaxation time as a function of the treatment of the NMR tube surface. If regular washing with water/ethanol/acetone already gives a T_1^{g} on the order of 20 minutes, by treating the tube wall with the piranha solution, T_1^{g} values of about two hours can be reached. The Surfasil coating [20] after these two steps can lead to T_1^{g} on the order of 4.5 hours (Fig. 4). After several pumping cycles, degradation of the surface coating is observed. Long relaxation times can be restored by renewal of the surface treatment.

3.2 Laser polarized ^{129}Xe $\longrightarrow$ ^{1}H cross-relaxation

Due to cross-relaxation, the presence of dissolved laser-polarized xenon, which is a spin system at very low positive or negative spin temperature, induces modification of the polarization of the m spins, I^k, that were initially at thermal equilibrium with the lattice [31]. Noting $\mathbf{Q}$ the vector of dimension 2^m containing any proton spin-order coherences of the kind $2^l \prod I_z^k$, and neglecting the heteronuclear cross-correlation, the spin dynamics is governed

by the equation:

$$\frac{\mathrm{d}}{\mathrm{d}t}\begin{pmatrix}\mathbf{Q}\\ S_z\end{pmatrix}=\begin{pmatrix}\mathbf{R} & \boldsymbol{\Sigma}\\ {}^t\boldsymbol{\Sigma} & \frac{1}{T_1^l}\end{pmatrix}\begin{pmatrix}\mathbf{Q}-\mathbf{Q}_0\\ S_z-S_0\end{pmatrix} \quad (1)$$

where $\mathbf{Q}_0$ is $\mathbf{Q}$ at thermal equilibrium, $\mathbf{R}$ is the homonuclear $2^m \times 2^m$ relaxation matrix, whose elements can be found for instance in reference [32], and $\boldsymbol{\Sigma}$ is a vector of dimension 2^m, whose m first elements are equal to the heteronuclear dipolar cross-relaxation rates σ_{I^kS} and whose other elements vanish. Finally T_1^l is the self-relaxation time of dissolved xenon. For the remainder of the text we shall refer to the $(2^m+1)\times(2^m+1)$ relaxation matrix as $\mathbf{R}'$. The presence of the term $\mathbf{Q}_0$ in equation (1) prevents a direct extraction of heteronuclear cross-relaxation from one experiment. However by acquiring two experiments with the same mixing time τ_m, but different initial conditions:

$$S_z^1(0) \neq S_z^2(0) \quad (2)$$

$$\mathbf{Q}^1(0) = \mathbf{Q}^2(0) \quad (3)$$

and performing a proton difference spectroscopy, one obtains:

$$I_z^{k\,1}(\tau_m) - I_z^{k\,2}(\tau_m) = \exp(-\mathbf{R}'\tau_m)\Big|_{I^kS}\Big(S_z^1(0) - S_z^2(0)\Big). \quad (4)$$

Equation (4) reduces for short mixing time to:

$$I_z^{k\,1}(\tau_m) - I_z^{k\,2}(\tau_m) = -\sigma_{I^kS}\tau_m\Big(S_z^1(0) - S_z^2(0)\Big). \quad (5)$$

The low value of the xenon-proton cross-relaxation rate σ_{I^kS} [9,10,33] relative to any proton relaxation rates prevents the use of equation (5) except for very short mixing times, but then the signal is expected to be almost undetectable. For longer mixing times, since this rate is small relative to the proton-proton cross-relaxation rate $\sigma_{I^kI^l}$, except if $\omega_I\tau_c \simeq 1.12$, according to equation (4), the signal enhancements depend on all proton relaxation pathways, and hence the quantification is difficult. In the basic SPINOE sequence [9], a proton π pulse synchronized with the xenon π pulse is applied during the mixing time. In terms of cross-relaxation, this experiment is then similar to the QUIET approach [34], which allows one to determine its efficiency. The spin system is reduced to the two-spin system (I^k, S) for mixing times that are short relative to $1/\sigma_{I^kI^l}$. This is obviously more simple but is still difficult to exploit. Increasing the number of π pulses seems not suitable due to possible artifacts. An attractive issue consists of eliminating the proton-proton cross-relaxation $\sigma_{I^kI^l}$ by off-resonance rf irradiation at the correct angle θ_I^0 between the static and the effective magnetic field direction in the rotating frame [35]. This angle is chosen so that the transverse relaxation compensates for the longitudinal one; obviously this method can only be used for $\omega_I\tau_c > 1.12$. In fact, as discussed in the general case in reference [32], all derivations (Eqs. (1–5)) can immediately be extended to the case of proton irradiation, since it only affects the relaxation rates and the term $\mathbf{Q}_0$, which is no longer the value at thermal equilibrium, but becomes the steady-state one. The effect of the rf irradiation on the xenon-proton cross-relaxation is to multiply the rate by a factor $\cos\theta_I^0$, which ranges between $\sqrt{2/3}$ (case of a big molecule) and 1. This solution reduces the efficiency of the polarization transfer by slowing down the heteronuclear cross-relaxation rates and by also increasing the proton self-relaxation rate. It, however, presents the advantage of avoiding the polarization transfer from xenon to a particular proton to be spread by spin-diffusion to many others. Moreover, if homonuclear cross-correlation can safely be neglected, the time dependence of the signal enhancement of any proton I^k generally given by equation (4), can be obtained simply by considering it as a two-spin system (I^k, S).

3.3 An improved SPINOE pulse sequence

The principle of difference spectroscopy with modification of the xenon spin-state is applied in the SPINOE experiment [9]. However we found that this pulse sequence gives peaks even in the absence of xenon, and so needed to be improved. Indeed, in any difference spectroscopy, peaks observed can be due to variations of chemical shifts, peak amplitudes or phases. The protocol we use for our SPINOE experiments consists of freezing the polarized xenon in the NMR tube above the evacuated solution *via* an hollow spinner filled with liquid nitrogen. The tube then reaches the ambient temperature in a few seconds in the fringe field of the NMR magnet. Vigorous shaking to introduce fresh laser-polarized xenon in solution precedes the introduction of the tube into the NMR magnet. This last operation can also be repeated before any SPINOE experiment. Consequently the problems that can occur are: (i) bad subtraction due to saturation of the analogic/digital converter, (ii) temperature change and/or inhomogeneity, (iii) temporal and/or spatial variation of the magnetic susceptibility, (iv) probehead mismatching and (v) radiation damping.

The last three problems are solved by the use of frequency-sweep adiabatic pulses on the xenon channel in the presence of a gradient pulse [36]. Inverting the xenon magnetization at the beginning of the mixing time every other FID makes the condition $S_z^2(0) \simeq -S_z^1(0)$.

The influence of possible temperature fluctuations as well as magnetic susceptibility variations on the chemical shifts are first tested in the absence of polarized xenon. Moreover a constant delay (30 s) is maintained between the introduction of the sample inside the magnet and the beginning of the SPINOE experiment. This period is sufficient to tune and match the probehead circuit, and to avoid field homogeneity losses due to bubbling.

Obtaining a constant proton spin state (Eq. (3)) at the beginning of the mixing time is not as obvious, because (1) the xenon magnetization is not at Boltzmann equilibrium and so influences the proton coherences, and (2) the accumulation of the SPINOE signal requires an interscan delay short relative to the xenon ${T_1}^l$ and also possibly

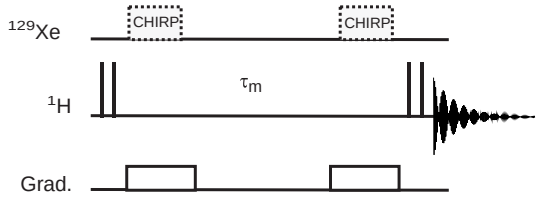

Fig. 5. One of the pulse sequences used to observe laser-polarized ^{129}Xe–^{1}H cross-relaxation. The thin bars represent 90° proton hard pulses. They are applied by pair with 90° phase shift in order to provide a better stability (composite pulse [37]). The xenon inversion is performed by an adiabatic frequency sweep pulse (CHIRP [38] of 1 ms) synchronized with a pulsed field gradient [36] of about 5 G/cm. This inversion is applied twice, in order to avoid variation of the nuclear magnetic susceptibility during the acquisition and xenon signal losses due to diffusion [36]. The difference spectroscopy is obtained by omitting the xenon CHIRP pulses every other FID. During the mixing time τ_m, an off resonance rf irradiation on the protons with adiabatic rotations at its ends [39] can be applied.

short relative to the self-relaxation time of the proton spin system. The solution chosen to obtain $\mathbf{Q}^1(0) = \mathbf{Q}^2(0)$ in the sequence of reference [9] is to saturate the protons, which is unfortunately difficult to setup for a scalar coupled proton system at high field. As shown by equation (4) saturation is not required, so in the sequence of Figure 5, the initial conditions can simply consist of a composite 90° hard pulse to avoid the effects of proton pulse miscalibration [37] followed by a strong pulsed field gradient. This makes $\mathbf{Q}^1(0) \simeq \mathbf{0}$ and is sufficiently stable to have $\mathbf{Q}^1(0) = \mathbf{Q}^2(0)$ after a few dummy scans. Another efficient and stable solution consists in saturating the proton magnetization by fast succession of phase-shifted 90° hard pulses, each followed by a pulsed field gradient of arbitrary value.

Finally to vary the influence of the ^{1}H–^{1}H cross-relaxation, either proton π pulses synchronized with xenon inversion or a proton off-resonance rf irradiation can be applied during the mixing time.

With all these precautions, the pulse sequence of Figure 5, is stable for mixing times up to 1.5 s to a level better than 0.1%.

3.4 Laser polarized ^{129}Xe ⟶ ^{1}H cross-relaxation in water

The two observations reported in the literature of cross-relaxation between laser-polarized xenon and protons of a cage-molecule dissolved in an organic solvent represent two extreme situations. The first one [9] is α-cyclodextrin in DMSO-d6, for which the previously reported binding constant with xenon is very low (2 M^{-1} at 298 K) [40]. The second one [10] treats more extensively the case of cryptophane-A in $1,1,2,2$ tetrachloroethane-d2, where a slow exchange with a binding constant greater than 3000 M^{-1} at 278 K and a xenon chemical shift variation of about 160 ppm were reported [41].

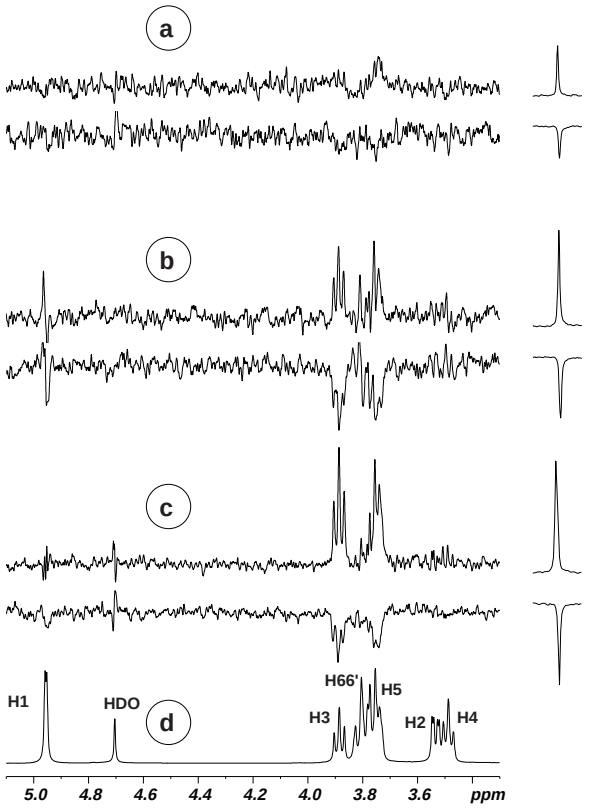

Fig. 6. (a–c), left: 500 MHz ^{129}Xe → ^{1}H SPINOE sub-spectra for α-cyclodextrin in D_2O for increasing mixing times (a: 150 ms; b: 300 ms; c: 600 ms). Right: corresponding ^{129}Xe signal obtained after a $\sim 1°$ read pulse (acquisition done just before the SPINOE experiment). For each mixing time, the two sub-spectra correspond to the results obtained with laser-polarized xenon produced with opposite direction of the magnetic field during optical pumping (lower trace: positive spin temperature). A constant scaling of the proton and xenon intensities has been kept. (d) 500 MHz ^{1}H spectrum of α-cyclodextrin with signal assignment ($T = 298$ K).

α-cyclodextrin is a cage-molecule composed of 6 glucose units linked in $\alpha 1-4$. This molecule has a truncated cone shape and is highly soluble in water and able to bind hydrophobic guests. It forms a complex with xenon in water with a binding constant on the order of 20 M^{-1} at 298 K [40]. The correlation time at 288 K is measured to be 0.48 ns using the method described in reference [32]. Considering a proton-proton distance of 3 Å (distance between H2 and H3), the longitudinal cross-relaxation rate at 11.7 T and 298 K is estimated to −0.01 Hz, which is small relative to what is encountered in a protein. This system consequently represents a convenient model for the SPINOE experiment in water.

Figure 6 presents sub-spectra obtained with our modified SPINOE experiment on a sample composed of 0.6 mg of lyophilized α-cyclodextrin dissolved in 350 μl D_2O ($C = 1.8$ mM) acquired at 11.7 T and 298 K (medium size wall NMR tube). From top to bottom, the sub-spectra correspond to increasing mixing times (a: 150 ms; b: 300 ms; c: 600 ms). Two sets of experiments are presented,

corresponding to two samples of laser-polarized xenon. The sign of their xenon polarization is opposite, as the direction of the magnetic field applied during optical pumping is reversed. Obviously we have checked that absolutely no peak appears in the absence of xenon (not shown). The phase of the proton SPINOE spectrum and that of the corresponding ^{129}Xe peak (right) have been voluntarily represented identical for sake of clarity, even if, as experimentally observed, the negative sign of the ^{129}Xe magnetogyric ratio leads to a 180° phase difference between the SPINOE spectra and the ^{1}H proton thermal equilibrium spectrum for a positive xenon spin temperature. Moreover from one line to another, no additional phase correction has been applied. Finally no important lack of resolution (which could be expected in such experiments) compared to the thermal equilibrium ^{1}H spectrum displayed in Figure 6d is observed, since, for instance, scalar couplings are well resolved.

In Figures 6b and 6c two in-phase peaks corresponding to the cyclodextrin H3 and H5 protons are clearly visible. These protons are located inside the cavity and are consequently expected to present the strongest interactions with the complexed xenon. Among the experiments 6a–6c, the best result is obtained for $\tau_m = 600\,\mathrm{ms}$ (Fig. 6c negative xenon spin temperature), which corresponds to the largest xenon signal, but also to a mixing time that is not too short relative to the average proton self-relaxation time ($T_1 \simeq 1.2\,\mathrm{s}$). In this experiment, the intensity of the SPINOE signal ($I_z^{k\,1} - I_z^{k\,2}$) of H3 relative to its signal after 600 ms of relaxation ($I_z^{k\,1} + I_z^{k\,2}$) is on the order of 1.9%, *i.e.* more than one order of magnitude larger than the stability level of our modified SPINOE experiment. For the experiment of Figure 6, the NMR tube contained a pressure of about 1.2 bar of isotope enriched (96%) xenon with an estimated polarization of about 15%. Not shown here, another successful experiment has been performed on the same molecular system at 288 K and 14 T using and not using off-resonance rf irradiation during the mixing time. Three bars of isotope enriched xenon with a polarization on the order of 7% served for this SPINOE experiment with an α-cyclodextrin concentration of 5 mM. All these experiments represent an enhancement of the xenon signal by about two orders of magnitude relative to the previously reported attempt to detect ^{129}Xe–^{1}H cross-relaxation in α-cyclodextrin in water [33]. As a consequence, to obtain a SPINOE signal that can be distinguished from artifacts or thermal noise, the present study reveals that it is unavoidable to resort to xenon polarization above 5% and either isotope enrichment or pressures above 2 bars.

The absolute intensity scaling both for proton and for xenon in Figures 6a–6c gives a good idea of the difficulty of a direct quantification of the SPINOE interaction, as the proton peak intensities depend not only on the mixing time, but also on the xenon magnetization, which is obviously not a constant value. Nevertheless in an attempt to go further in the quantification procedure, after correction of the proton SPINOE peak intensities by the corresponding xenon signal, we have measured magnetization build-up curves for both sets of experiments. The relaxation rates, summarized in Table 1, are expressed in relative units rather than in $\mathrm{Hz\,mM^{-1}}$, to avoid large uncertainties resulting from the lack of precision in the xenon magnetization measure. The results reveal a good agreement between the two sets of experiments. The difference in the cross-relaxation rate values given between the left and the right columns correspond to a 2% error for the Xe–H3 distance and 1.5% for Xe–H5. The average Xe–H3 distance is 7% bigger than Xe–H5, allowing *via* triangulation the determination of the average location of the noble gas atom inside the cavity. Even if proton-proton cross-relaxation is expected to have a relatively weak influence for this system, in Figure 6c top trace, protons H2 and H4 can be discerned. Their intensities are larger than expected for a direct xenon-proton cross-relaxation if one assumes that dipolar contribution arises only from xenon located inside the cavity. Indeed they lead to Xe–H2 and Xe–H4 distances which are 1.5 and 1.4 times bigger than Xe–H3 while any molecular model would conclude that the distance ratios are about 2. This illustrates how spin-diffusion can alter the direct quantitative interpretation of SPINOE experiments, especially as the observation of these intermolecular interactions needs long mixing times.

Table 1. Xenon-proton cross-relaxation rates extracted from Figure 6 for positive and negative xenon spin temperature. The rates are expressed in Hz for a xenon magnetization equal to that of Figure 6c top trace. The uncertainties on the rates derived by using equation (5) are on the order of 10% and principally result from the intensity error on the data at 150 ms, which is on the order of 50%.

proton	Xenon spin temperature positive	negative
H3	4.6×10^{-3}	4.0×10^{-3}
H5	4.9×10^{-3}	5.3×10^{-3}

4 Conclusions

An experimental setup designed to prepare laser-polarized xenon for liquid-state NMR applications is described. It allows the preparation, in regular NMR tubes, of samples with pressure up to 4 bars of laser-polarized xenon with a useful polarization inside the spectrometer above 5%, while most of the similar applications range between 1 and 2% polarization [33,43]. Thanks to surface coating of the NMR tubes very long self-relaxation times (around 4.5 hours) are measured for gaseous xenon.

This laser-polarized xenon has been used in SPINOE experiments modified to avoid artifacts resulting from transient effects, pulse miscalibration, radiation damping and nuclear susceptibility changes. The stability of this new implementation and the high xenon nuclear polarization enable the first direct observation of a polarization transfer between laser-polarized xenon and protons of a solute molecule in water where xenon solubility is low. This study shows that observation of proton signal enhancement requires very large xenon magnetization and

then strong constraints on the production. As a consequence, firstly new gas transfer conditions towards the liquid NMR sample should allow us to increase the useful xenon magnetization. Secondly, since polarization above 5% is required, we are trying to improve our average xenon polarization in two complementary directions: (i) by using a new solenoid design to prevent signal losses during the condensation; (ii) by characterizing the optimal pumping conditions (nitrogen and xenon pressures, temperature and pumping duration) thanks to the systematic use of an home-built CW spectrometer working *in situ*. Still, this approach opens the way to the study and the characterization of hydrophobic cavities using dissolved laser-polarized xenon. As already pointed out [10], the derivation of structural information from xenon-proton cross-relaxation rates will become problematic for large molecules such as proteins due to spin-diffusion. One of the solutions, which is under evaluation in our laboratory and already seems promising, consists in the cancellation of proton-proton cross-relaxation thanks to a proton off-resonance rf irradiation.

In the development of this experiment we have been advised by Jean-Claude Berthet for the choice of the glassware, Claude Fermon for the coils design, Gérard Francinet for diverse electronic devices, Pascal Leverd for handling the rubidium in a glove box, and Vincent Huc and Serge Palacin for coating the glassware surfaces. They are all colleagues from CEA/Saclay. We thank them warmly. We finally acknowledge Lucy Bull for a careful reading of this manuscript.

References

1. Y. Montet, P. Amara, A. Volbeda, X. Vernede, E.C. Hatchikian, M.J. Field, M. Frey, J.C. Fontecilla-Camps, Nat. Struct. Biol. **4**, 523 (1997).
2. F. Venema, Ph.D. thesis, Katholieke Universiteit Nijmegen, 1996.
3. B.W. Matthews, A.G. Morton, F.W. Dahlquist, Science **270**, 1847 (1995).
4. J.A. Ernst, R.T. Clubb, H.X. Zhou, A.M. Gronenborn, G.M. Clore, Science **270**, 1848 (1995).
5. G. Otting, E. Liepinsh, B. Halle, U. Frey, Nat. Struct. Biol. **4**, 396 (1997).
6. E. Liepinsh, P. Sodano, S. Tassin, D. Marion, F. Vovelle, G. Otting, J. Biomol. NMR **15**, 213 (1999).
7. K. Inoue, H. Yamada, T. Imoto, K. Akasaka, J. Biomol. NMR **12**, 535 (1998).
8. G. Tastevin, H.-U. Kauczor, *Hyperpolarized gases in magnetic resonance: Biomedical investigations and clinical applications,* International workshop: June 21 – 25, 1999, Les Houches, France.
9. Y.-Q. Song, B.M. Goodson, R.E. Taylor, D.D. Laws, G. Navon, A. Pines, Angew. Chem. Int. Ed. English **36**, 2368 (1997).
10. M. Lühmer, B.M. Goodson, Y.-Q. Song, D.D. Laws, L. Kaiser, M.C. Cyrier, A. Pines, J. Am. Chem. Soc. **121**, 3502 (1999).
11. H.L. Clever, *IUPAC Solubility Data Series* (Pergamon Press, Oxford, 1979).
12. M.A. Bouchiat, T.R. Carver, C.M. Varnum, Phys. Rev. Lett. **5**, 373 (1960).
13. W. Happer, Rev. Mod. Phys. **44**, 169 (1972).
14. W. Happer, E. Miron, S. Schaefer, D. Schreiber, W.A. van Wijngaarden, X. Zeng, Phys. Rev. A **29**, 3092 (1984).
15. T.G. Walker, W. Happer, Rev. Mod. Phys. **69**, 629 (1997).
16. G.D. Cates, D.R. Benton, M. Gatzke, W. Happer, K.C. Hasson, N.R. Newbury, Phys. Rev. Lett. **65**, 2591 (1990).
17. D. Raftery, T. Long, T. Meersmann, P.J. Grandinetti, L. Reven, A. Pines, Phys. Rev. Lett. **66**, 584 (1991).
18. B. Driehuys, G.D. Cates, E. Miron, K. Sauer, D.K. Walter, W. Happer, Appl. Phys. Lett. **69**, 1668 (1996).
19. M.P. Augustine, K.W. Zilm, Mol. Phys. **89**, 737 (1996).
20. X. Zeng, E. Miron, W.A. van Wijngaarden, D. Schreiber, W. Happer, Phys. Lett. A **96**, 191 (1983).
21. B. Driehuys, G.D. Cates, W. Happer, Phys. Rev. Lett. **74**, 4943 (1995).
22. R.L. Gamblin, T.R. Carver, Phys. Rev. A **138**, 946 (1965).
23. G.D. Cates, S.R. Schaefer, W. Happer, Phys. Rev. A **37**, 2877 (1988).
24. T. Rõõm, S. Appelt, R. Seydoux, E.L. Hahn, A. Pines, Phys. Rev. B **55**, 11604 (1997).
25. H.J. Jänsch, T. Hof, U. Ruth, J. Schmidt, D. Stahl, D. Fick, Chem. Phys. Lett. **296**, 146 (1998).
26. U. Ruth, T. Hof, J. Schmidt, D. Fick, H.J. Jänsch, Appl. Phys. B **68**, 93 (1999).
27. L. Darasse, G. Guillot, P.J. Nacher, G. Tastevin, C.R. Acad. Sci. Paris IIb **324**, 691 (1997).
28. F. Kober, P.-E. Wolf, J.-L. Leviel, G. Vermeulen, G. Duhamel, A. Delon, J. Derouard, M. Décorps, A. Ziegler, Magn. Reson. Med. **41**, 1084 (1999).
29. F. Kober, B. Koenigsberg, V. Belle, M. Viallon, J.-L. Leviel, A. Delon, A. Ziegler, M. Décorps, J. Magn. Reson. **138**, 308 (1999).
30. M. Gatzke, G.D. Cates, B. Driehuys, D. Fox, W. Happer, B. Saam, Phys. Rev. Lett. **70**, 690 (1993).
31. G. Navon, Y.-Q. Song, T. Rõõm, S. Appelt, R.E. Taylor, A. Pines, Science **271**, 1848 (1996).
32. H. Desvaux, P. Berthault, Prog. NMR Spectrosc. **35**, 295 (1999).
33. A. Stith, T.K. Hitchens, D.P. Hinton, S.S. Berr, B. Driehuys, J.R. Brookeman, R.G. Bryant, J. Magn. Reson. **139**, 225 (1999).
34. C. Zwahlen, S.J.F. Vincent, L. Di Bari, M.H. Levitt, G. Bodenhausen, J. Am. Chem. Soc. **116**, 362 (1994).
35. H. Desvaux, P. Berthault, N. Birlirakis, M. Goldman, J. Magn. Reson. A **108**, 219 (1994).
36. P. Berthault, H. Desvaux, G. Le Goff, M. Pétro, Chem. Phys. Lett. **314**, 52 (1999).
37. R.R. Ernst, G. Bodenhausen, A. Wokaun, *Principles of nuclear magnetic resonance in one and two dimensions* (Clarendon Press, Oxford, 1987).
38. J.-M. Böhlen, M. Rey, G. Bodenhausen, J. Magn. Reson. **84**, 191 (1989).
39. H. Desvaux, P. Berthault, N. Birlirakis, M. Goldman, M. Piotto, J. Magn. Reson. A **113**, 47 (1995).
40. K. Bartik, M. Lühmer, S.J. Heyes, R. Ottinger, J. Reisse, J. Magn. Reson. B **109**, 164 (1995).
41. K. Bartik, M. Lühmer, J.-P. Dutasta, A. Collet, J. Reisse, J. Am. Chem. Soc. **120**, 784 (1998).
42. A.L. Davis, G. Estcourt, J. Keeler, E.D. Laue, J.J. Titman, J. Magn. Reson. A **105**, 167 (1993).
43. C.R. Bowers, V. Storhaug, C.E. Webster, J. Bharatam, A. Cottone III, R. Gianna, K. Betsey, B.J. Gaffney, J. Am. Chem. Soc. **121**, 9370 (1999).